JOURNAL OF GUIDANCE, CONTROL, AND DYNAMICS
Vol. 19, No. 5, September–October 1996

# High-Performance Active Control of Dynamically Complex Space Structures

D. J. Phillips,* J. A. King,† L. D. Davis,* and D. C. Hyland‡
*Harris Corporation, Melbourne, Florida 32902-9400*

**Experimental results obtained in a multiyear program to assess the cost and benefits tradeoffs of active structural control for precision space structures are reported. The combination of a complex segmented optics structural test article with broadband disturbances and very stringent performance requirements on both line-of-sight and higher-order aberration errors resulted in an exceptionally challenging control task, involving over 20-dB attenuation of dozens of vibration modes within the 10–200-Hz disturbance band. The authors applied a variety of control design techniques together with two distinct suites of vibration control actuator hardware. The control challenge, the actuator hardware designs, and the remarkably successful experimental results pertaining to a baseline decentralized control design are described.**

## I. Introduction

IN recent years, a variety of large experimental facilities have been made available for the study of identification and control of space structures.[1–4] Among such experimental activities, the ACTS program was a multiyear effort to assess the cost and complexity vs performance tradeoffs of active vibration control on precision space structures. This program was limited to intrinsically active vibration suppression approaches. Neither passive approaches nor active devices that mimic passive approaches were considered.

To conduct the assessments, the ACTS program posed an extremely challenging control problem using a large-scale, traceable (to future missions) structural test bed, termed the structural test model (STM), that was provided and operated by an independent host contractor. The control problem was addressed by guest contractor teams (one of which was constituted by the authors) who attempted experimental demonstrations of high-performance control systems. In particular, guest contractors designed and fabricated controls hardware and designed control algorithms, all space qualifiable and consistent with realistic mission constraints, and supported test activities at the STM facility. The host contractor presided over test executions and data acquisition. This arrangement, which is similar to the completed NASA Controls-Structures Interaction Guest Investigator Program,[5,6] makes for an independently refereed experimental program with results subject to independent corroboration.

The STM, which emulates the dynamics of a segmented optical system, is described in Sec. II. Together with its performance requirements, the STM constitutes what is very probably the most challenging vibration control problem yet addressed by the structures and controls community. Stringent performance requirements are levied not merely on line-of-sight (LOS) error but also on higher aberration errors, e.g., rms wave front errors, to which over a hundred vibration modes contribute. In the presence of broadband disturbances exciting over 150 modes in the 10–200-Hz band, these specifications mean that the response of dozens of vibration modes must be attenuated by at least 20–40 dB.

The activities reported here to address the ACTS control challenge spanned three years (November 1991 through December 1994). The fundamental development and test approach, described in Sec. III, used a step-by-step building up process that gave performance data on a large number of totally distinct control approaches—involving distinct types and combinations of hardware and control algorithms of widely varying complexity.

In particular, in terms of hardware, this study used two different types of actuators to address the ACTS problem. The first to be applied were the linear precision actuators (LPACTs). These devices apply frequency-dependent damping forces to the structure by accelerating a proof mass mounted on a spring using an electronmagnet. These actuators were not placed in the load path of the structure, and demonstrated the results possible with a bolt on retrofit system. Second to be applied were the active isolation fittings (AIFs), which are intrastructural devices employing a piezocrystal that is commanded to expand and contract to absorb the motion of the base body (typically a spacecraft bus) without transmitting the motion to the payload. In contrast to most other approaches, the AIF maintains high static stiffness, even when deactivated, thus achieving isolation while maintaining the inherent rigidity needed to achieve rapid retargeting. In addition, these devices reduce vibration both at major resonances of the system and between resonances. The LPACT and AIF designs and their associated decentralized control systems are described in Secs. IV and V, respectively.

LPACTs and AIFs were tested both separately and together and, in each case, a succession of control algorithms of increasing complexity was investigated ranging from decentralized to modern multivariable designs. Although a great deal was learned about the complexity vs performances tradeoffs of modern multivariable design approaches (including many surveyed in Ref. 7), we confine attention here to the decentralized control results. These designs are the simplest, most readily applicable in a realistic mission scenario and are comparable in performance to centralized multi-input/multi-output (MIMO) designs in any case. Although the lessons learned from more complex approaches will be reported separately, Sec. VI describes the experimental results of decentralized control with LPACTs and AIFs, both operating separately and together.

The results shown here exhibit an unprecedented degree of broadband vibration suppression. The performance metrics typically show peak attenuations of over two orders of magnitude and across broad frequency ranges. All evidence of resonant phenomena is eliminated. Moreover, the hardware and algorithm designs are highly robust, fault tolerant, and traceable to mission constraints. Finally, all results were achieved with modest resources within a disciplined development schedule. In view of these features, the results reported here established a new benchmark for the state of the art in vibration control for precision space structures.

## II. Control Challenge: STM Facility, Performance Goals, and Open-Loop Test Data

In this section we describe the STM test bed for the ACTS program and the associated control problem.

Received July 25, 1995; revision received Jan. 10, 1996; accepted for publication March 4, 1996. 

*Staff Engineer, Government Aerospace Systems Division, P.O. Box 94000, MS 19/4825.
†Lead Engineer, Government Aerospace Systems Division, P.O. Box 94000, MS 19/4825.
‡Senior Scientist, Government Aerospace Systems Division, P.O. Box 94000, MS 19/4825. Member AIAA.

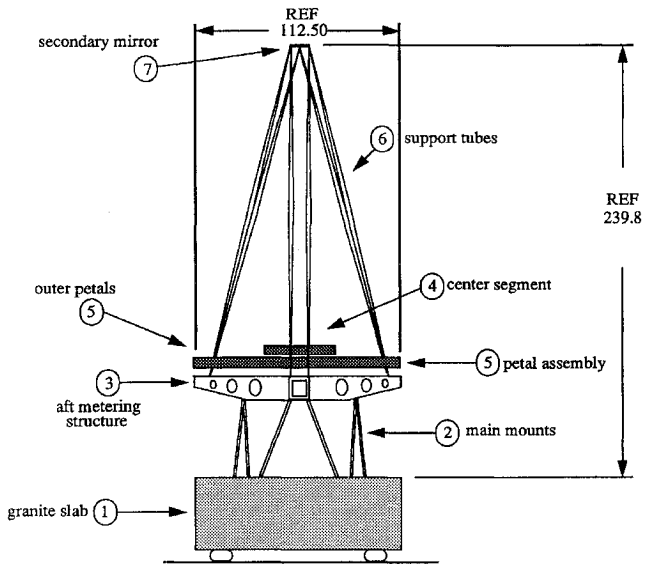


**Fig. 1 Side view of the ACTS STM test bed.**

The STM (see Fig. 1) consists of a graphite epoxy aft metering structure, which supports a center segment simulator and six petal assembly simulators. It is a mechanical model that is representative of generic segmented optical systems that may be adapted quasistatically in space. No polished optical surfaces are used. Instead, mass simulators replicate the inertial properties of optical elements that would be used in an optical system.

Figure 1 shows the main features of the mechanical system: the granite slab 1, the main mounts 2, the aft metering structure 3, the center segment simulator 4, the petal assembly simulator 5, the support tubes 6, and the secondary mirror assembly (SMA) simulator 7. The aft metering structure is supported by six main mount struts and in turn provides a platform to connect the six support tubes that hold the SMA simulator in position. The support tubes, main mounts, and aft metering structure are each made from graphite epoxy, whereas the center segment and petal assembly simulators are aluminum. The SMA simulator is a two piece stainless-steel weldment.

The center segment simulator weights 141 lb. Each of the petal simulators weighs 95 lb. The total weight of the STM excluding the slab is approximately 1000 lb, whereas the slab weighs 28,500 lb. As shown, the height of the STM is approximately 20 ft, its diameter approximately 10 ft at its widest point.

The disturbance inputs to the system are provided by two shakers attached to the granite slab. One shaker is mounted on top of the slab and is used to excite the slab in the $Z$ (vertical) direction. The $Z$ shaker is used as a proof mass actuator and is controlled via an accelerometer mounted on the proof mass. The other shaker is floor mounted and is connected to the granite slab using a stinger with an integral force transducer. It excites the slab in the $X$ (horizontal) direction.

The nominal disturbance spectrum is a shaped spectrum in the band from 10 to 200 Hz, and results in an rms input force of approximately 82.2 lb. Although the actual force spectrum applied has notches to compensate for large resonances in the shaker yokes and in the granite slab, the net effect on the structure is a smooth spectrum over the 10–200-Hz band, which results in an rms base acceleration of approximately $2.8 \times 10^{-3} g$.

Since only two shakers ($X$ and $Z$) are available for input, there remains the problem of estimating what the effects of a $Y$ input would be. For this, one assumes the structure is symmetric, and takes the $Y$ LOS motion resulting from an input in the $X$ direction as equivalent to motion in the $X$ direction resulting from inputs in the $Y$ direction. Hence, for example, the net $X$ LOS motion resulting from inputs in all three directions is estimated as the root sum square (rss) of the $X$ motion resulting from an input in the $X$ direction, the $Y$ motion resulting from an input in the $X$ direction, and the $X$ motion resulting from inputs in the $Z$ direction. For wave front error and defocus estimates, response to inputs in the $X$ direction is root mean squared twice with the response to inputs in the $Z$ direction to obtain the result.

The performance scoring system is independent of any control system and is operated by the host contractor in its role as referee. There are three sets of scoring accelerometers: primary mirror assembly, secondary mirror assembly, and instrument assembly. Scoring accelerometers provide an inexpensive, rugged method for performance evaluation with sufficient resolution over the 10–200-Hz band to discern compliance with the performance goals.

The primary mirror assembly accelerometers are mounted on top of the mirror segment simulators, directly above the mounting interfaces for the segment support struts. There are 3 such accelerometers per segment, for a total of 21 on the primary mirror assembly. Their sensitive axes are directed toward the center of curvature of the primary mirror, which is located above the secondary mirror assembly. This allows the scoring system to discern tip, tilt, and piston (vertical displacement) for each segment, assuming they remain rigid as individual segments. There are three secondary mirror assembly accelerometers mounted at the top of the SMA support strut interface points. Their sensitive axes are directed at the center of curvature of the secondary mirror.

Finally, a set of three accelerometers is mounted near where an instrument package would be located for the optical system. They provide accelerations in the $x$, $y$, and $z$ directions.

The performance scoring system uses a least squares best fit of the primary mirror accelerometers (with outputs double integrated to yield position estimates) with a nominal paraboloid to obtain net dynamic pointing error, defocus, and higher-order wave front error resulting from primary mirror motion. The secondary mirror and instrument assembly accelerometers are also used to assess pointing error and defocus of the system relative to inertial space. The computations are evaluated in the frequency domain over the 10–200-Hz band to obtain the performance metrics to be described.

Performance goals for vibration attenuation are given in terms of three primary measures: LOS error, defocus, and wave front error. The LOS performance metric $J_1$ is based on an integral in the frequency domain of the single-sided power spectral density (PSD) of the inertial LOS angle $S_\theta(f)$ where $f$ is the frequency in hertz and $S_\theta$ is expressed in scaled units, here called cells. $J_1(f)$ is approximately $\sqrt{8}$ times the rms LOS error occurring within a $\pm$ 5% bandwidth of the current frequency. Thus it smoothes out very rapid changes in the PSD of the inertial LOS. The precise definition is

$$J_1(f) = \sqrt{\frac{8 I_1(f)}{2\pi f}}$$

where

$$I_1(f) = \int_{0.95f}^{1.05f} (2\pi u)^2 S_\theta(u)\, du$$

$J_1$ is specified in both the $X$ and $Y$ directions. $J_{1x}$ is the motion of the LOS pointing vector component in $X$, or the rotation about the $Y$ axis. $J_{1y}$ is defined analogously. The requirement is that in the closed loop $J_{1x}$ and $J_{1y}$ fall below the frequency-dependent bound shown in Fig. 2. This is discussed later in connection with open-loop performance.

Defocus is defined as the vertical distance between the actual focal point and the sensor plane. The originally specified requirement was 0.1-mil rms (2 sigma) over the band of 10–200 Hz. Later, this requirement was recognized to be entirely unrealistic and a goal of 2-mil rms (1 sigma) over 10–200 Hz was recommended.

Wave front error (WFE) is defined as the higher-order (excluding the defocus component) rms optical pathlength deviations over the aperture. The wave front error goal is specified in terms of the total rms over the band from 10 to 200 Hz. It is 0.04 waves, 2 sigma. Assuming a constant PSD level for the wavefront error, a level PSD of $2.1 \times 10^{-6}$ waves$^2$/Hz would be required over the band of 10–200 Hz.

To appreciate the severity of these requirements, we show open-loop test data for the principal performance metrics in Figs. 2–4.

The $J_1$ performance of the open-loop system is shown in Fig. 2 (because the $x$ and $y$ components are similar, only the $y$ component is shown); the dashed line indicates the corresponding $J_1$ performance goal. Note that approximately 20 dB of attenuation is required in the

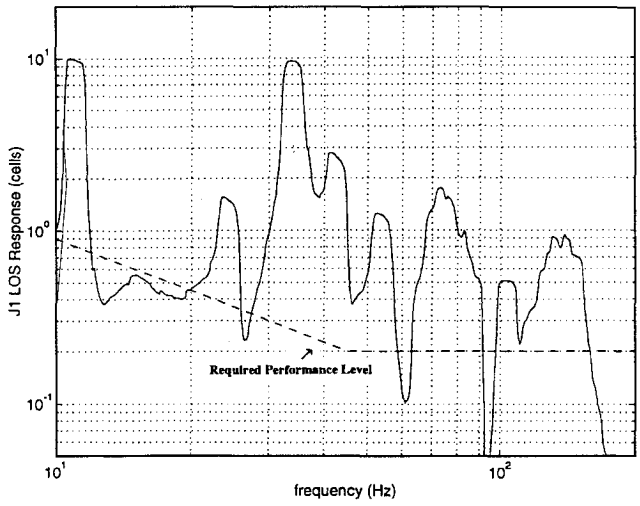


**Fig. 2 Typical $J_{1y}$ open-loop performance.**

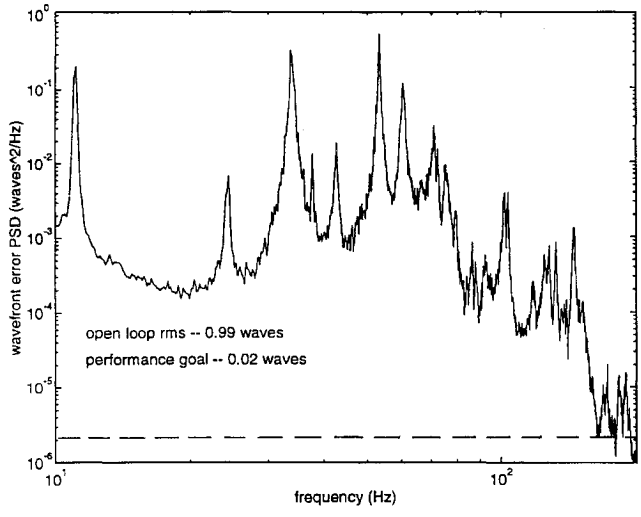


**Fig. 3 Typical WFE open-loop performance.**

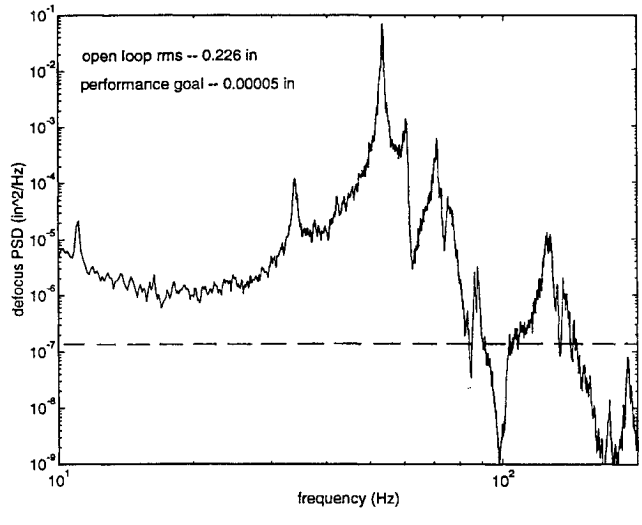


**Fig. 4 Typical defocus open-loop performance.**

region of 11 Hz and approximately 30 dB in the region of 35 Hz. The peak at 11 Hz is the result of 14 separate modes: the 12 first local modes of the SMA support tubes and the 2 first cantilever bending modes of the SMA tower acting as a unit. Also, note the smoothing effect of the $I_1$ integration on the modal behavior. The peaks of the modes throughout the band have been smoothed (lowered), so that the actual attenuation of individual modes required is more than indicated in the figure (approximately 50 dB on the 35-Hz modes). Also, the number of significant modes excited is large (~200) and spreads throughout the 10–200-Hz band.

The open-loop wave front PSD is shown in Fig. 3. Note the open-loop rms level of 0.99, which compares with a goal of 0.02, 1 sigma. This is a broadband attenuation requirement of 36 dB. Note the numerous large modal spikes, the largest of which appears at 34 Hz and must be attenuated 56 dB to attain the mean PSD level corresponding to the rms performance goal.

Special emphasis should be given to the wave front error, because it is actually composed of 18 independent degrees of freedom (DOF) (21 sensors on the primary mirror assembly minus the overall tip, tilt, and piston of the best fit system). The reduction of this single quantity requires the attenuation of vibration over all seven mirror segments simultaneously, and is not amenable to control by means of simpler correction schemes such as active steering mirrors.

Finally, the defocus PSD of the open-loop system is shown in Fig. 4. It has several major peaks, with the most significant occurring at approximately 52 Hz. Even the more modest, revised performance goal of 2-mil rms over 10–200 Hz would require 33 dB of rms attenuation over 10–200 Hz and 56 dB of attenuation of the 52-Hz mode.

In summary, the ACTS problem is easily the most challenging vibration attenuation problem so far posed to our knowledge.[1–6] It is wideband, encompassing hundreds of lightly damped modes (both local and global). It requires large attenuations, which means the control system must function over large dynamic ranges. Finally, it penalizes vibration both in terms of low-order distortion such as LOS and defocus, and higher-order distortion in the form of WFE.

## III. Control System Development Procedure and Overall Control Architecture

The three-year ACTS program effort was designed with three major goals: 1) achieve the performance goals just described, 2) clarify the value and costs associated with different control strategies and design methods, and 3) demonstrate the effectiveness of LPACT and AIF devices on the STM. This paper emphasizes results pertaining to goals 1 and 3.

To achieve these goals, we adopted an approach to control design, implementation, and test validation that may be called gradualism[8] because it is predicated on the idea that the best results are achieved in easily understood increments of complexity. It is the result of extensive experience in the laboratory. Fundamentally, it is a methodology for designing control systems that combines algorithm design, system modeling, and subsystems and component testing into a realistic strategy for implementation. It progresses step by step from simple control algorithms to more complex and coordinated control algorithms and from simple control subsystem hardware elements toward the integration of all hardware elements. While exploiting the capability of advanced controls design methods where appropriate, the methodology allows a flexible response to unforeseen contingencies and to new modeling data.

Two layers of gradualism are present in a program such as ACTS. The first of these involves the hardware subsystems, which are first treated separately before being integrated as a single, monolithic system. In ACTS these two subsystems consist of the LPACT inertial proof-mass actuators and the AIFs. In addition to the reduced complexity of initial separate treatment, this stepwise approach to control system integration allows the assessment of the relative contribution made by each subsystem to overall system performance.

The second layer of gradualism is perhaps the more important of the two. It determines how the control system for a given set of hardware is developed and demonstrated. The process for development can be roughly split into five stages: architecture definition, open-loop testing, rate feedback (positive real) design, decentralized design, and advanced centralized design. When properly executed, this process yields a set of designs of incrementally increasing performance and complexity, which can be traded to obtain an optimum compromise.

The first stage of control systems design is the architecture definition, which usually must occur before the system to be controlled is actually built. It generally makes use of analytical models such as a finite element model. The projected disturbance environment and the desired performance metrics are applied to estimate the performance

of the uncontrolled system. Given the open-loop data (ideally correlated with experimental data), the structural design of the system, the available sensor and actuator technologies and the implementation constraints, the designer determines the number, placement, and requirements of the control system components. In the present instance, two sets of collocated actuators and sensors were selected. In most cases, the architecture definition is the most important factor affecting the performance ultimately achieved by the system.

Once the control hardware is obtained, it is integrated into the system, and open-loop testing is performed using the actuators as exciters and sensors as receptors. In addition, disturbances are applied and measured with the sensors. This allows control system algorithm design to proceed not with idealized models of the system but with actual test data including all of the vagaries of the hardware.

The next step, which can often be carried out along with the open-loop testing, is to apply a very simple, non-model-based control scheme such as rate feedback. Such schemes are guaranteed to work under broad conditions and are often capable of achieving the lion's share of performance ultimately achieved by practical control systems.

The fourth step makes use of the test data obtained from the open-loop and simple closed-loop testing to design a more refined decentralized system consisting of a number of single-input/single-output loops. The individual loops may be synthesized as linear combinations of actuators and sensors. A variety of techniques may be used for each loop synthesis, including direct frequency-domain classical design. The advantage of this step is that it forces the designer to understand the physics of the system and allows the individual tailoring of each loop using designer insight. The idea is to improve the performance of the already functional, decentralized, non-model-based controller.

The last step is to develop a controller using advanced (e.g., multivariable, optimization-based, state–space) techniques that coordinate the operation of the actuators and sensors of a given subsystem, or that connect the elements of different subsystems together. This last step is taken based on the design and demonstration data developed in the previous steps, and its complexity must be justified based on the predicted performance improvement. In many cases, this last step entails prohibitive increases in design cost and implementation complexity.

Since it involves several incremental steps of design and demonstration, the gradualist methodology naturally depends more on measured results and less on rosy pretest predictions than a single modeling-design-implementation-test cycle. In each step of the process, designs were arrived at a priori and tested on site under the inspection of the host contractor. This process gives performance data on a large number of distinct control approaches—with varying complexity and distinct types and combinations of hardware.

The repeated exposures to the structural hardware entailed by the described plan is consistent with normal processes in major development programs. First, many, if not most, major development programs include the development of one or more engineering test beds prior to production. Several well-planned visits to the test bed, followed by a single test session on the production hardware, are a reasonable scenario in the context of such a program. On the other hand, the various test visits may be compared to operational periods of a production system. Improvements are introduced over the life of the program at block changes, based on previous experience and well-substantiated analysis. This kind of gradualism is common in long-standing, high-valued programs. Either way, the development strategy shown here is analogous to those of many successful operational programs.

The plan, including several on-site test sessions, was carried out within budget and with no significant schedule deviations. Performance data on many different types of control designs were obtained. Centralized, multivariable designs produced modest improvements over the decentralized designs but at the expense of significantly increased complexity and design development cost. Whereas the applicability of multivariable, optimization-based methods on problems of extreme complexity such as that of ACTS will be treated in extenso in separate publications, this paper discusses only the decentralized designs and the associated experimental results. The next two sections describe the separate LPACT and AIF subsystem hardware designs and associated decentralized control loops. Section VI presents test results for the LPACT subsystem alone, the AIF subsystem alone, and both subsystems operating simultaneously.

## IV. LPACT Control Subsystem

The LPACT,[9,10] depicted in Fig. 5, is a voice coil driven proof-mass actuator wherein the proof mass is suspended on flexures thereby obviating the need for linear bearings. By commanding current through the voice coil windings, a magnetic field is created which interacts with a permanent magnetic field from a magnet on the pole piece. This interaction causes the proof mass (pole piece) to accelerate, thus creating a reaction force on the structure to which the actuator is mounted.

The LPACT uses a highly accurate servoaccelerometer mounted on the proof mass as part of an analog control loop, which not only damps the spring-mass resonance of the flexure proof-mass system but also reduces the effects of nonlinearities. This loop is referred to as the force loop because it ensures that the actuator behaves as a force actuator within its bandwidth.

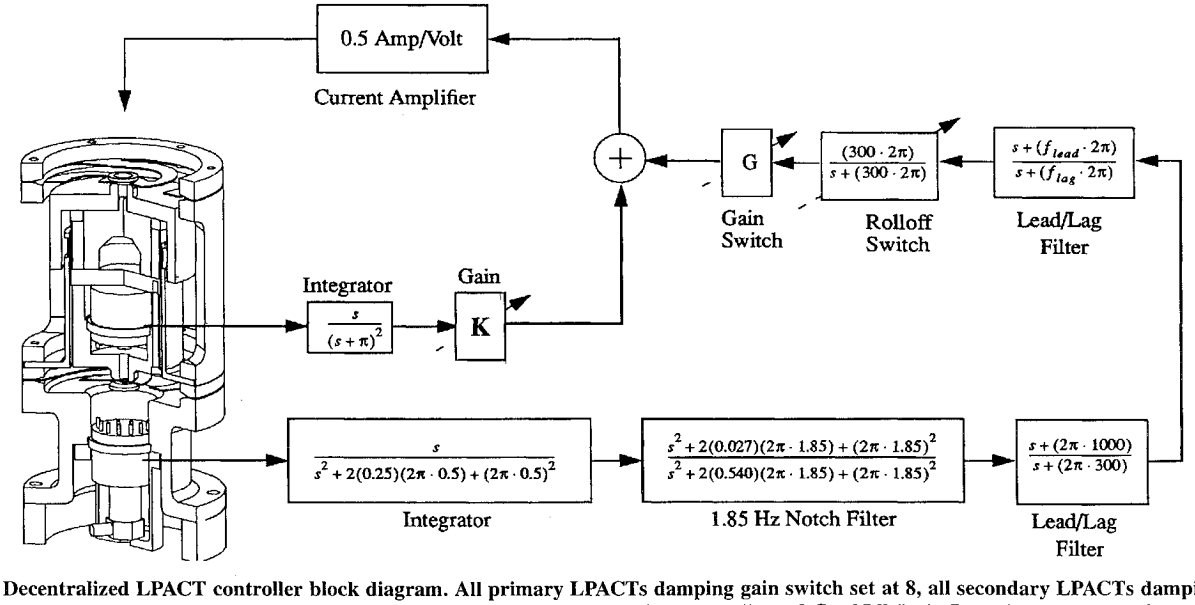


**Fig. 5 Decentralized LPACT controller block diagram. All primary LPACTs damping gain switch set at 8, all secondary LPACTs damping gains switch set at 4, and no digital control is used. Primary LPACTs: $f_{lead}$ = 15 Hz, $f_{lag}$ = 0.01 Hz, and $G$ = 25 lb/in./s. Secondary LPACTs: $f_{lead}$ = 16.6 Hz, $f_{lag}$ = 6.0 Hz, and $G$ = 8 lb/in./s.**

Two chassis mounted accelerometers, a lower bandwidth servo type and a high bandwidth piezoresistive type, are also used. The two accelerometer signals are combined via a crossover network to form a hybrid accelerometer, which provides a wide bandwidth, collocated acceleration measurement at the actuator site. This measurement is then passed through analog signal conditioning, which includes a pseudointegrator and other simple compensation, which may be required based on the specific application, to form an analog rate-feedback control loop. The result is a sensor-actuator pair, which can provide analog rate feedback with bandwidths up to 1–2 kHz. Since the velocity measurement is with respect to inertial space, the damping added by the rate feedback is also with respect to inertial space. As a result, with the rate feedback loop closed, the LPACT acts as an inertial damper (i.e., a dashpot connecting the structure to a fixed location in inertial space).

In addition, the supporting electronics for the LPACT provide an interface so that a digital control loop can be placed in parallel to the analog rate-feedback loop. The rate estimate derived from the hybrid accelerometer measurement can be used as a control measurement and a D/A command from the computer can be summed into the force command to the actuator. As a result, the LPACT can conceivably be commanded by three control loops at once: the force loop using the proof-mass mounted accelerometer, the analog damping loop using the combined chassis mounted accelerometers, and a digital loop, which may either be local or part of some centralized controller using more than one LPACT.

We first summarize the steps taken to define the requirements of this subsystem (including sizing, placement, and orientation of the actuators), then describe the final design with its decentralized control loops.

**Requirements of LPACT Subsystem**

Initial finite element model (FEM) based analysis indicated an open-loop wave front error of 1082-nm rms compared to the performance goal of 6 nm. This and open-loop LOS results indicated that active control needed to provide 40 dB of broadband attenuation to achieve desired results. In consideration of dynamic range, force output, displacement, and noise issues, it was determined to require 20-dB attenuation capability from the LPACTs and an additional 20-dB attenuation from the AIF subsystem. This requirement strongly drives the selection of LPACT numbers, sizing, and placement.

Before the actuator sizing and design tasks could be performed, it was of course necessary to decide on the number of actuators to be used, as well as their structural location and orientation.

All initial analysis was done using a comprehensive finite element model of the structure, which also included the isolation airbags and the granite slab. This highly detailed model was provided by the host contractor and had been correlated with test data up to approximately 100 Hz.

The method for evaluating a given actuator configuration consisted of frequency-domain analysis assuming ideal rate feedback at each actuator site and then applying the prescribed slab disturbance force spectrum. The subsequent closed-loop frequency response functions at the truth sensor locations, combined with the base disturbance PSD, were then processed to give LOS and primary surface quality performance predictions. A rate feedback control can be viewed as a general MIMO dynamic compensator with most of its parameters constrained. Obviously, upon the imposition of constraints, the value of a minimum (e.g., the minimum of a quadratic performance penalty) cannot decrease. Hence, from the point of view of achievable attenuation vs required actuator effort, rate feedback is a worst case (relative to refined decentralized or centralized designs) and is, therefore, used as the basis of sizing decisions.

To narrow the number of possibilities to a more manageable size, we decided on the number of actuators to be used and their locations based on a number of simple, practical constraints (described later), and then varied the orientations to finalize the configuration.

Because the aluminum petal simulators are a simplified represention of a multilayer assembly that would actually consist of the optical surface, positioning elements, and a stiff backup structure, it was not possible to emulate precisely how LPACTs would be installed on the real system. The LPACTs would be placed on the support structure beneath the optical surface, not intruding on the optical characteristics, but providing damping to the structure directly beneath it. In the absence of an optical surface, the aluminum petals were viewed as the backup structure for a theoretical optical surface mounted above them. Given that the frequency range of the disturbance and performance is so large (10–200 Hz), the best way to attenuate vibration on the petals is to oppose the disturbance forces being transmitted through the petal mounts, rather than placing actuators elsewhere on the petals. Thus, since there are seven petals, each having three mounting points, 21 actuators would be necessary on the primary surface. Based on experience on an in-house test bed,[11,12] the required placement scheme involves three actuators placed near the secondary surface mounting points. In summary there are a total of 24 actuators and a set of reasonable locations.

The next step was the selection of the orientations of the petal-mounted actuators. Alignment of the three secondary platform actuators along the sides of an equilateral triangle in the $x-y$ plane was evaluated and found to be quite satisfactory. Orientations of the petal-mounted actuators posed more difficult issues. LOS and WFE suppression capabilities were evaluated for four orientation schemes. In addition, we considered the optimal selection of orientations with a gradient descent algorithm using the rms WFE as the performance criterion. Results from the optimization algorithm were disappointing because of the large number of local minima and the apparent difficulty in obtaining good performance simultaneously on WFE and LOS. In fact, one of the orientation schemes designed via engineering judgment proved clearly superior to all other candidates and was adopted. This is the configuration shown in Fig. 6. In this arrangement, each of the three actuators on a petal is tilted 45 deg from the $x-y$ plane, and the vertical plane containing the actuator axis passes through the midpoint of the chord joining the locations of the other two actuators sharing the same petal. The horizontal component of the actuator orientations is essential for performance improvement near 35 Hz. This is because the structural response at 35 Hz is dominated by a mode in which the mount struts act like cantilevered beams fixed at the slab and the structure above the main mounts translates in the $xy$ plane as a rigid body. With a rate-feedback control design, the selected orientations shown in Fig. 6 proved capable of an order of magnitude LOS and WFE improvement with rate feedback gains of 150 lb/in./s for the primary LPACTs and 15 lb/in./s for the secondary LPACTs.

These analyses were revisited using detailed models of the LPACT dynamics, accelerometer dynamics, and more realistic designs for the analog rate-feedback control loops. The latter design included a pseudointegrator to derive a rate estimate from the accelerometer, a notch filter to stabilize the airbag modes near 2 Hz, and lag-lead compensation to ensure positive reality above ~10 Hz. This refined analysis showed that acceptable performance could be

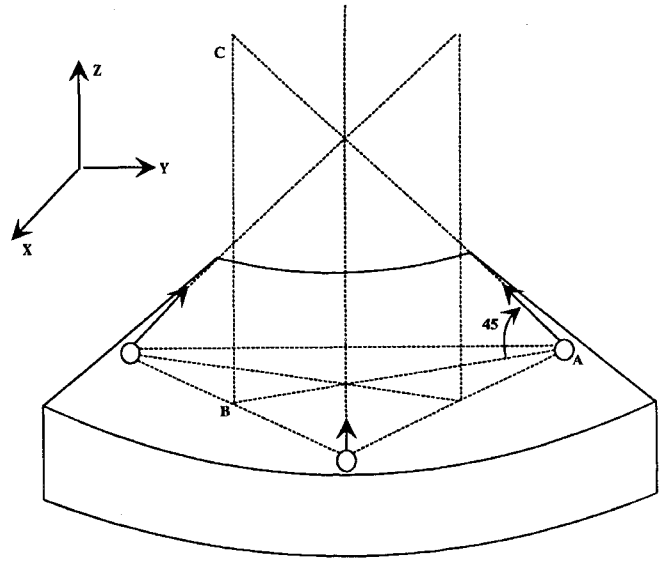


**Fig. 6 Selected LPACT mounting locations and orientations on each primary mirror petal simulator panel.**

**Table 1 Comparison of LPACT predictions vs test results**

| Parameter | Predicted | Measured |
|---|---|---|
| Resistance, Ω | 5.5 | 5.5 |
| $Bg$, T | 0.44 | 0.41 |
| Force constant, N/A | 7.08 | 6.0 |
| Inductance, H | 0.9e-3 | 0.9e-3 |
| Resonant frequency, Hz | 5.5 | 5.5 |
| Proof-mass weight, lb | 1.23 | 1.23 |

achieved with in-band damping gains lowered to 50 and 10 lb/in./s for the LPACTs on the primary and secondary, respectively.

Next, given the rate-feedback dynamics as designed, the amount of force required from each LPACT was computed. To formulate the final sizing requirements, we applied a factor of 3 to the worst-case actuator site to get a peak force and an additional factor of 2 for conservatism. The resulting required force and mass-stroke product were 10-N peak force and 0.0025-kg-m mass-stroke. These formed the basic inputs to the LPACT computer-aided design package, which also imposes additional practical constraints (total mass, physical envelope, etc.) to finally provide design drawings from which LPACT prototypes can be fabricated.

After several runs of the automated design code, the best design was selected, fabricated, and then tested. Test results for this prototype are given in Table 1, where $Bg$ denotes the gap flux density. Both analytical predictions and actual tested values are shown.

The analytical predictions matched closely with the test results. Measured frequency response functions of the prototype with the force loop closed showed that the gain was flat (within 3 dB from 3 to 1000 Hz) and the actuator had only 25 deg of phase lag at 1000 Hz. This phase lag was primarily a result of the current loop bandwidth of the servoamplifier. This prototype exceeded all of the design specifications and was approved as the design for the 26 LPACTs (including two spares) for the STM.

Total LPACT force noise was an additional important issue addressed. Because of the low vibration levels being sought, a prediction of the force output of the LPACTs resulting from electrical noise was made to ensure that the noise floor of the actuators was well below the desired closed-loop force output of the actuators. First, a detailed model of the LPACT and signal conditioning electronics was constructed using the nominal design values arrived at during the actuator sizing process. The output of this model was the applied force on the structure. The inputs were the accelerations at both the accelerometer on the proof mass, as well as the chassis-mounted accelerometers.

This model, together with a model of the accelerometer noise PSD, was used to predict the total PSD of the LPACT forces on the structure resulting from noise. This LPACT noise output model was verified on the prototype using a special vibration-isolated test rig. These results showed that structural response levels because of LPACT noise are several orders of magnitude below the desired closed-loop levels. Hence, we concluded that LPACT force noise is acceptably low.

#### Decentralized LPACT Control Design

The decentralized control design for the LPACT subsystem arose from two different objectives. Early in the program, before detailed modeling data were obtained, it was developed to achieve significant closed-loop results with a highly robust controller. Later, even after highly detailed models were available, the decentralized controller was perfected to achieve a design that is applicable to a generic class of structures (of which the STM is a representative example) with little or no modifications to accommodate detailed structural characteristics. In connection with the latter objective, the control system was required 1) to maintain stability and performance despite arbitrary structural parameter uncertainties in all modes above 10 Hz and 2) to minimize the complexity of actuator to sensor interconnections to facilitate implementation and checkout. During checkout testing one must be prepared to inspect every actuator-to-sensor transfer function. This and related considerations mean that implementation cost rises rapidly with the number of sensors interconnected with each actuator through the controller. Hence, this number must be minimized. Both requirements 1 and 2 very strongly motivate a positive real design with independent control loops for each LPACT, using a velocity estimate from the casing-mounted accelerometer. With ideal rate measurements and ideal inertial actuators, constant feedback gains result in a strictly positive real controller. This, together with the strictly positive real plant, guarantees stability regardless of structural modeling errors.[13–16] To arrive at the final decentralized design, this simple scheme was modified to account for various nonideal conditions, i.e., high-frequency LPACT and accelerometer dynamics, and low-frequency LPACT and slab dynamics.

These refinements are shown in Fig. 5, which shows the final decentralized design and the components of the force loop. Here, however, we discuss the structural control loop, which uses the casing mounted accelerometer (the lower loop in Fig. 5). This control loop is purely analog and uses a velocity estimate formed by integrating the accelerometer output. The constant gains were determined by FEM-based analysis and the performance requirements. Although the LPACT casing accelerometer combination exhibits little phase or gain variation up to 1000 Hz, the control must still be rolled off to prevent instabilities involving very high-frequency structural modes. The strategy is to add a one pole rolloff filter that allows the control loop to retain positive reality up to 200 Hz, while providing enough rolloff to gain stabilize the very high-frequency modes beyond 200 Hz. Initial open-loop tests in the 200 Hz–1 kHz range established the minimum dissipation of high-frequency modes. This information was used to select the rolloff corner frequency (300 Hz) to ensure adequate gain margin. In addition, a lag/lead filter was used to shape the gain and phase characteristics of the loop at the upper bandwidth boundary.

The remaining refinements in Fig. 5 are designed to compensate for low-frequency dynamics in the LPACTs and the granite slab support system. All of these characteristics are manifested below the lowest STM structural frequencies (~11 Hz) and are amenable to precise modeling through simple analysis and straightforward subsystem testing. A lag/lead filter is used to provide phase lag in the neighborhood of 10 Hz to offset some of the phase lead associated with the rollup of the LPACT dynamics. Finally, a 1.85-Hz notch filter is used to gain stabilize some of the granite slab/airbag modes.

## V. AIF Subsystem

In contrast to the LPACT, which applies external, inertial loads to the structure, the AIF is an intrastructural device. That is, it operates as a primary load-bearing part of the structure and alters the structure's dynamic behavior to sharply reduce the transmission of vibration to the isolated body. The AIF is illustrated by the drawing in Fig. 7, and its principles of operation have been described in Ref. 17. It consists of four main parts: the piezoactuator, which lengthens and shortens the fitting according to the applied voltage; the top accelerometer, which senses the motion at the base of the isolated body; the bottom accelerometer, which senses the disturbance motion of the base body; and the compensation electronics, which may be implemented with a combination of baseline analog components and augmented with digital controllers as appropriate.

This mix of inertial sensors with an intrastructural actuator is an unusual feature in active isolators. Most isolators operate by reducing the stiffness of the main mount, and then adding damping to the resulting, low-frequency main mount modes using some type of intrastructural actuator. The operation of the AIF is fundamentally different. It uses two control loops, termed here the top and bottom loops, to achieve good isolation without reducing static stiffness of the main mount. Each of the isolation control loops is described in greater detail as follows.

The top accelerometer loop attempts to zero out the motion of the top accelerometer by feeding it back directly to the piezocommand, using appropriate filtering. The total effect of the top loop is to stiffen the fitting at the top accelerometer, with the greatest stiffening occurring at the resonances, which cause significant deflection of the top accelerometer. The tendency of the top loop operating alone is to attenuate greatly any main mount resonances. Off-resonance isolation is usually achieved only in combination with the bottom accelerometer feedforward loop.

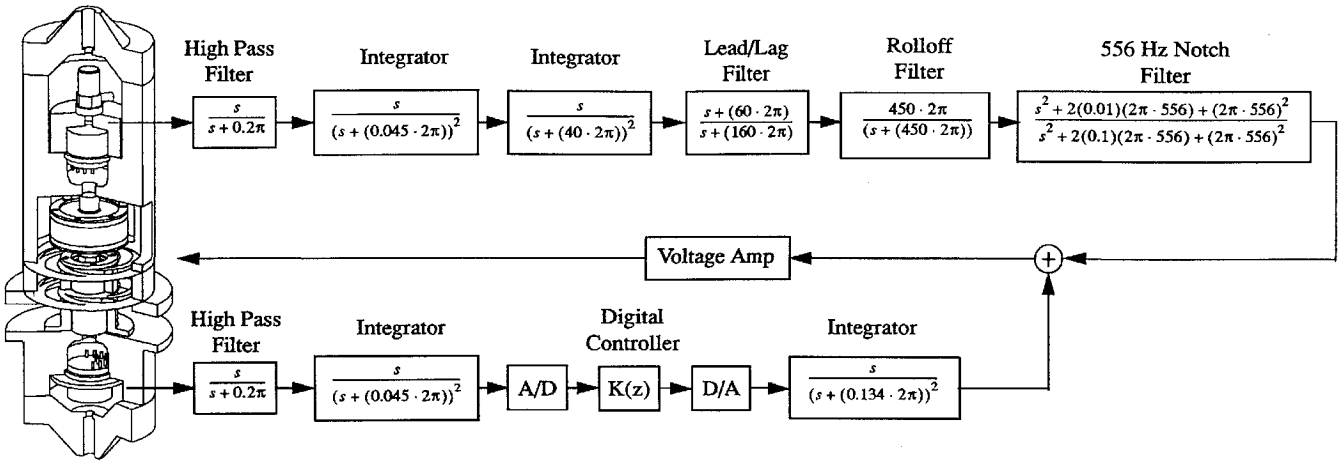


**Fig. 7 Block diagram of the active fitting configuration and its decentralized control system (closed local analog loop using top accelerometer and closed local digital isolation loop using bottom accelerometer).**

The bottom feedforward loop is intended to achieve isolation from base-induced disturbances by causing the piezocrystal to shrink and grow to exactly absorb the base motion in the band of interest. This is achieved by estimating the inertial displacement of the base along the axis of the fitting using the base accelerometer, and compensating for any gain or phase variations of the piezostack and accelerometer. Once this is achieved, large attenuations are possible in both resonant and nonresonant frequency regions.

To appreciate the basis for AIF robustness and stability, a refined analysis was provided in Ref. 17, which addresses the dynamics of the entire system, including AIF dynamics, loop compensators, the base body and isolated bodies. This shows that in the presence of ideal position estimates the entire system is equivalent to a unity feedback interconnection of a positive real system and a strictly positive real system. Of course, the idealized conditions of Ref. 17 can only be approximately realized over a finite frequency band because of accelerometer dynamics, the high-frequency dynamics of the piezoelectric stack actuator, and the use of realizable low-pass filters to form position estimates from the accelerometer output signals. As described subsequently, the top and bottom loop designs contain low-pass and lead-lag elements that compensate for these nonidealities so as to recover the ideal robustness properties within the desired isolation frequency band. These compensator designs depend only on dynamic characteristics of the AIF device itself and not on the adjoining substructures.

The combinatorial properties of positive real systems[13] imply that stability and performance of one AIF is not sensitive to the presence of other AIFs in the system, so that more complex isolators can be built up from independent AIF units. This applies when six AIFs are used together to form a six-DOF isolation mount with the important proviso that moment release flexures are placed at the ends of the members. This ensures that the only significant dynamic loads in the mount elements are axial. In addition, since only the axial load path is controlled, transmission of shear and bending moments must be kept to a minimum.

Each active fitting is controlled locally, independently of the others. Though no electronic communication occurs among the fittings, they all operate cooperatively to reduce the total disturbance transmitted to the load, in all six degrees of freedom.

The process of deciding where to place and how to orient the AIF actuators on the STM was simpler than that of the LPACTs because of the intrastructural nature of the actuators. There were really only three different locations to be considered: in the support-tube interface, the petal simulator mounts, and the main mounts. Placing AIFs between the primary surface and the secondary would only provide isolation for the secondary. This would not address the primary surface quality aspects of the control problem, nor would it likely solve the LOS problems since the motion of the primary would be effectively unchanged. Replacing existing petal simulator mounts with AIFs would be difficult because of space limitations. Given that the disturbances would be applied on the granite slab and would have to be transmitted through the main mounts, the obvious choice was to replace the existing main mounts with new struts which each included an AIF. In addition, the AIFs would be placed on the top end of the new struts, closest to the payload to prevent flexibility in the struts from amplifying residual disturbance forces on the isolated structure.

#### Requirements for the AIF Actuators

To determine the sizing requirements for the AIF actuators, the displacement of the granite slab and the accelerations experienced there were computed three ways: from the nominal problem goal disturbance spectrum, from the measured open-loop response resulting from inputs in the $Z$ direction, and from the measured open-loop response due to inputs in the $X$ direction. The maximum rms was used for each disturbance case.

Using the worst-case results of 3.3 mg and 0.030 mil and applying a factor of three to achieve peak values, as well as a factor of two for safety, we obtained a requirement of 0.18 mil of displacement and 20 mg of acceleration, 0 peak.

The bandwidth requirement for attenuation was set equal to the bandwidth of the performance specification, 10–200 Hz. Attenuation was defined as the ratio of the closed-loop rms displacement to open-loop rms displacement as seen at the interface between the top of the AIF and the isolated body. Attenuation is evaluated using a nominal disturbance spectrum, over the frequency band from 10 to 200 Hz. Based on the results from the preliminary LPACT system analysis, the residual performance improvements needed from the AIF system was approximately 20 dB. To specify the amount of attenuation needed by an individual AIF, the NASTRAN model was used to estimate the performance loss resulting from the coupling of the six support struts. This coupling was introduced by imperfect moment release at the strut interfaces. This analysis showed only a 3–6-dB loss in performance from the coupling. As a result, a conservative requirement for each fitting was 30-dB rms attenuation.

As a result of the sizing analysis, the accelerations at the AIF sites were known to be similar to those seen at the LPACT locations. The Sundstrand accelerometer, seen as the dominant noise source in the LPACT system, had been used in the development of the AIF prototype. It had been easily packaged and was the baseline for this application. Since the controller gains for both the LPACTs and the AIFs are similar (because the attenuation requirements are similar), as long as the same high-gain accelerometer amplification electronics were used, there would be no noise problems.

Detailed mechanical and electrical designs were completed so as to meet all of the requirements on stroke, bandwidth, and maximum loads. In addition, a static stiffness requirement was imposed such that the new AIF-mounted struts would maintain the stiffness of the original support struts on the STM. The motivation for this is the consideration that in the event of an actuator failure, the best active isolation system should revert to the nominal stiffness of a purely passive structure.

### Decentralized Control Design

The decentralized control for the active fitting subsystem is shown in Fig. 7. As noted earlier, two control loops are used. The first is purely analog and uses the top accelerometer. After gravity bias is removed via a high-pass filter, the accelerometer signal is used to form a position estimate via two integration filters. Next, the position estimate goes through a lead/lag filter and single-pole (450-Hz) rolloff filter. Finally, a notch filter is used to gain stabilize a particularly lightly damped mode at 556 Hz.

The other control loop uses the bottom accelerometer measurement to derive a feedforward position isolation loop, commanding the piezostack to shrink and expand so as to absorb the motion of the base. This loop employs analog and digital elements as shown at the bottom of the figure. Again, after having removed the gravity bias, the acceleration signal is passed through a digital controller $K(z)$ used to gain stabilize dynamics outside of the 10–200-Hz band while canceling the dynamics of the active fitting within the band. Finally, the digital controller output is passed through another integration filter, which not only smoothes the converted digital signal, but also ensures that the digital controller effectively uses a position measurement and generates a position command. The basic components for each $K(z)$ are a matching filter used to cancel sensor and actuator dynamics in the 10–200-Hz band while providing rolloff outside the band, and notch filters to gain stabilize those modes not gain stabilized by the rolloff. In addition to the matching filter, each $K(z)$ contains two notch filters at 554 Hz and 1.35 kHz used to gain stabilize two very lightly damped modes.

## VI. Closed-Loop Experimental Results for Decentralized Designs

In this section we present experimental results for the decentralized control subsystems described in Secs. IV and V. Results obtained for each subsystem individually and for both combined are discussed in separate subsections.

### LPACT Subsystem Performance

Figures 8–10 show the performance attained with the final LPACT system configuration operating alone. Here we show (in Fig. 8) only the PSD of the $Y$ LOS component, as the behavior of the $X$ component is very similar. Also, we defer discussion of the $J_1$ performance metric for the combined LPACT and AIF case. All of the figures show that significant damping has been added to the structure, especially below 100 Hz. Virtually no resonant behavior is evident in this frequency band. As expected from the characteristic loop transfer functions, less damping has been added above 100 Hz because of the lower amplitude of the higher frequency modal peaks.

Stability margins were generous for the final LPACT configuration. Typical LPACT loop transfer functions (with all other loops closed) show gain margins of 12 dB and never rise above a gain of 1.

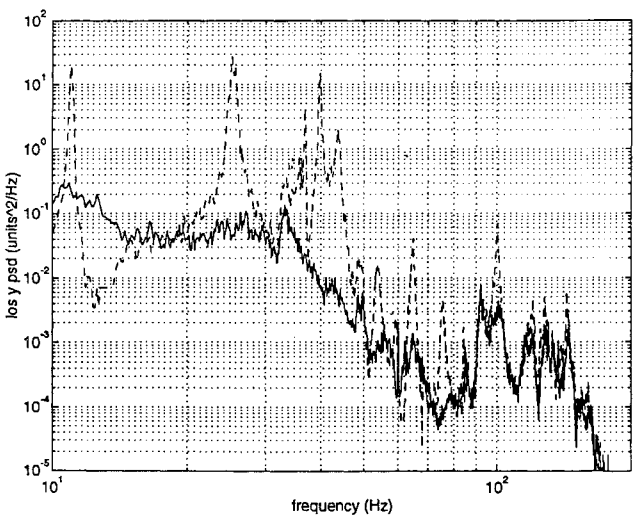


**Fig. 8 $Y$ LOS PSD results for the LPACT subsystem alone.**

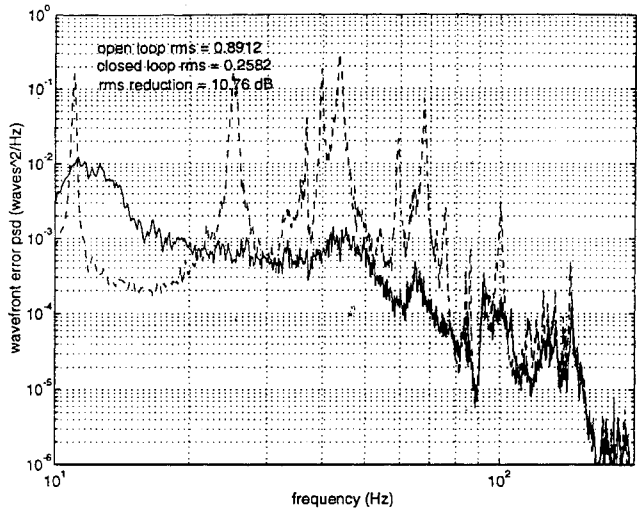


**Fig. 9 WFE results for the LPACT subsystem alone.**

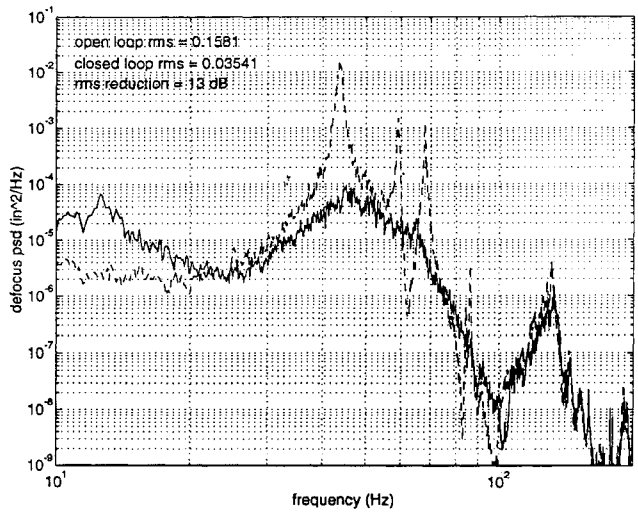


**Fig. 10 Defocus results for the LPACT configuration subsystem alone.**

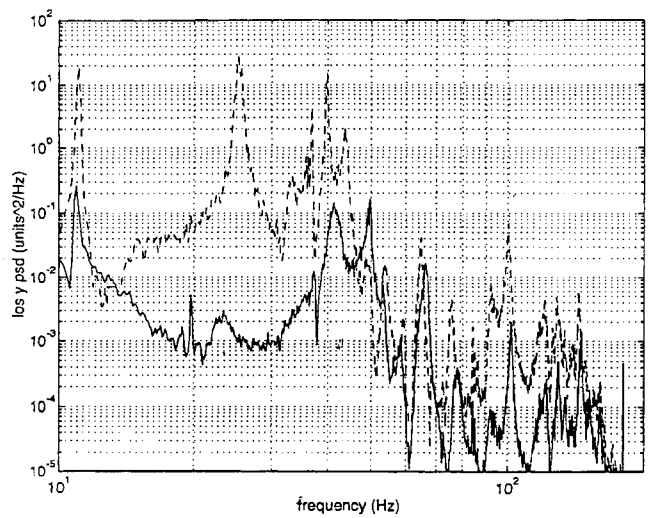


**Fig. 11 $Y$ LOS PSD results for the AIF configuration subsystem alone.**

Each actuator contributes only a modest amount of performance. It is the aggregate of all 24 that results in the impressive results shown.

### Active Fitting Subsystem Performance

Figures 11–13 show the performance for the final active fitting control system. The performance improvement is best from 10 to 50 Hz, where 20–40-dB reduction can be seen in all three performance measures. In a small neighborhood around 48 Hz, the performance

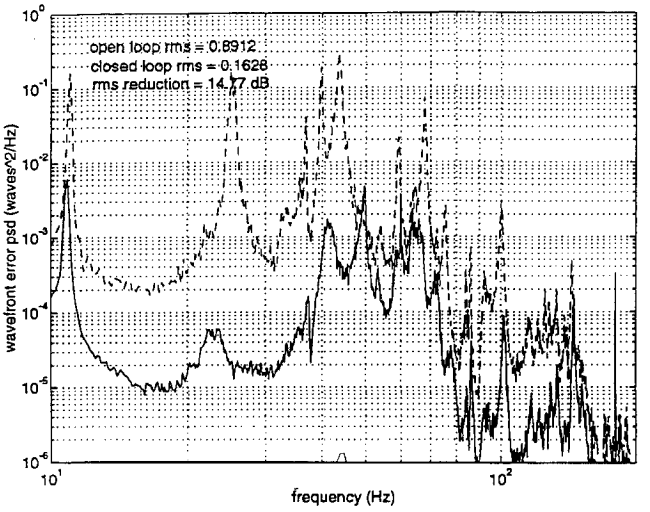


**Fig. 12 WFE results for the AIF configuration subsystem alone.**

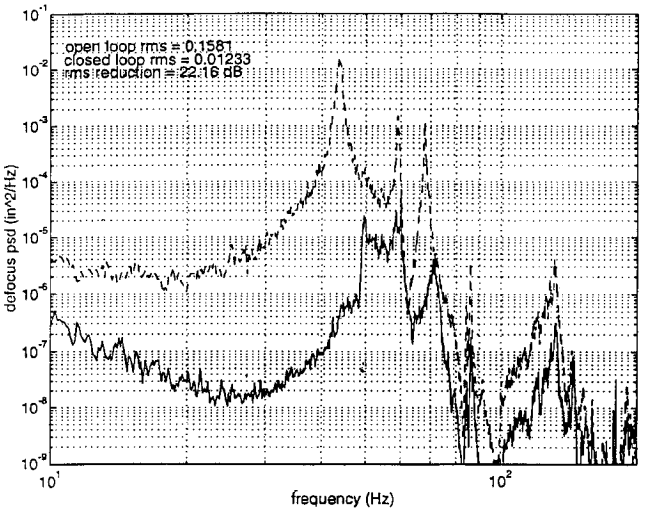


**Fig. 13 Defocus results for the AIF configuration subsystem alone.**

is either unchanged or slightly worsened. This has been traced to an unforeseen internal structual resonance in the AIF (which causes loss of attenuation over a narrow band) and is not attributable to the decentralized design strategy used here. From 55 to 200 Hz, performance improvement is 10–20 dB. The rms wave front and defocus improvements of 14.77 and 22.16 dB are somewhat better than those achieved by the LPACT system (10.76 and 13.00 dB), since lowering of the rms value beyond what the LPACT system achieved requires lowering of the nonresonant response, as well as the resonant peaks.

The stability margins for the AIF loops were lower than those for the LPACTs but are still above 5-dB gain margin.

### Combined LPACT/Active Fitting Control System Configuration

The combined system is formed merely by activating both control systems in the configurations already described. No further modifications were necessary, because the two subsystems were found to interact in a benign fashion. In particular, detailed examination was made of loop transfer functions for actuators in each subsystem, with and without the other subsystem activated. The data showed that the stability margins and performance of each subsystem were almost entirely unaffected by the other subsystem.

Figures 14–17 show the performance achieved with the final combined system. In addition to the LOS PSD in Fig. 14, Fig. 15 shows the corresponding $J_1$ result with the performance requirement. The closed-loop system more than meets the requirement over the whole band except for the narrow region around 50 Hz. This is because of the (remediable) AIF structural resonance already noted. The results are what one would expect when combining the performance of the two subsystems. The modal peaks have been reduced by the LPACT

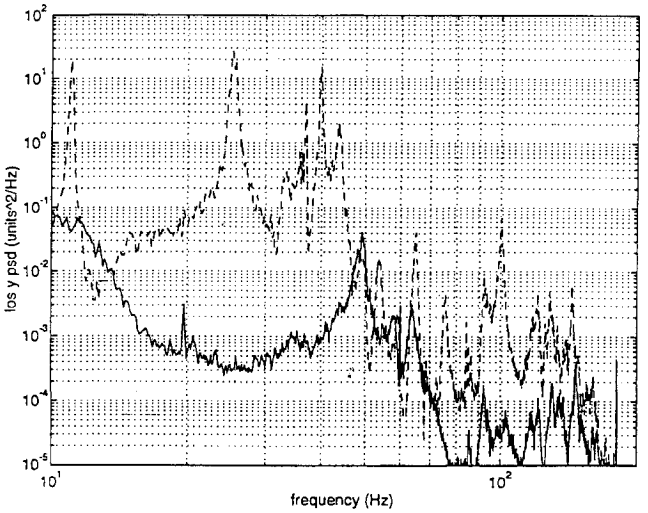


**Fig. 14 *Y* LOS PSD for AIFs and LPACTs combined.**

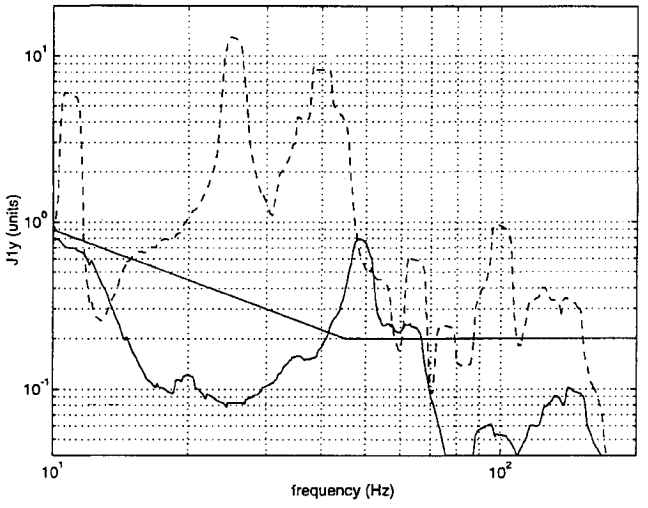


**Fig. 15 $J_{1y}$ results for AIF and LPACTs combined.**

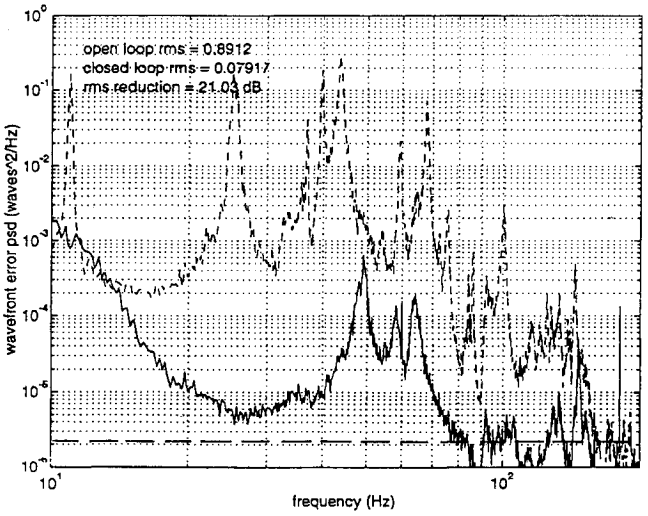


**Fig. 16 WFE results for AIFs and LPACTs combined.**

system, and the overall level of response (resonant and nonresonant) has been lowered by the active fitting system. In Fig. 14, note that the peak near 25 Hz, which represents a cluster of 12 modes, has been attenuated by over 40 dB. Other critical LOS modes have been attenuated by approximately 40 dB. The WFE has been improved by 21.03 dB, significantly more than the improvement achieved by either system alone. The defocus error has likewise been improved by 28.91-dB rms over the 10–200-Hz band and the dominant modal cluster near 42 Hz is attenuated by over 50 dB.

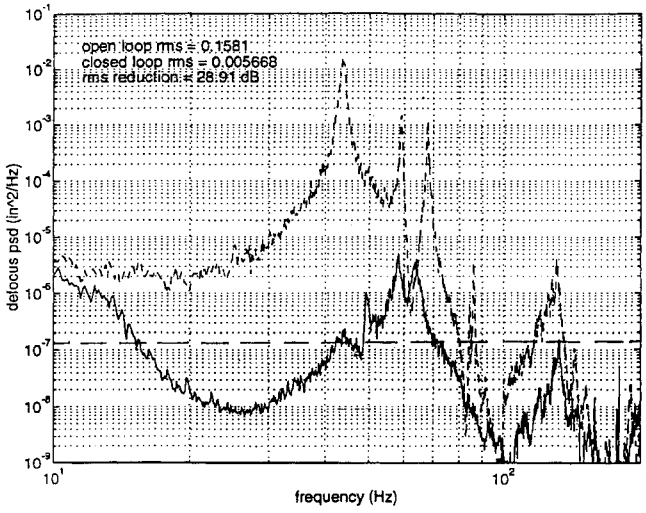


**Fig. 17 Defocus results for AIFs and LPACTs combined.**

## VII. Conclusions

This paper has summarized a multiyear effort to assess the costs and benefits of active vibration control for precision space structures. We sketched the experimental facility, the extremely challenging control problem, and the characteristics of the actuator and sensor hardware that was applied to the system. Although a range of control methodologies was tested, this paper was confined to a description of the decentralized control designs and the corresponding test results. Within the context of hardware development and decentralized design and test several useful lessons were gleaned, as follows.

1) The ultimate performance achievable with a given system is critically linked to its architecture. This fact was clearly shown in the architecture study task mentioned in Sec. III. Large variations in performance were seen (even with idealized actuators) with differences in actuator orientation alone. By using high-bandwidth, highly accurate actuators and sensors, which are located and oriented properly, the actual feedback controller can be greatly simplified. Another important consideration is the reasonable allocation of attenuation required by a given control system. By devising two separate control systems, each assigned to achieve approximately 20 dB of vibration attenuation, we ultimately achieved 30 dB of reduction with the two systems working together. The controllers that achieved this performance were very simple and easily understood. This layered approach is more attractive than the approach requiring 30 dB of attenuation from a single system.

2) The majority of achievable performance for a large MIMO structural control problem can be reached with decentralized control. As mentioned at the end of Sec. III, only modest improvements in performance were realized with the addition of centralized control (~6 dB in certain narrow-frequency ranges). This is not to say that centralized control is not capable of providing larger performance improvements when used on its own. The point here is that very substantial performance improvements (30–40-dB broadband) can be achieved with decentralized control. This is good news in terms of system robustness resulting from sensor or actuator failure, since with our decentralized scheme such failures lead only to graceful degradation of performance. Centralized schemes, on the other hand, typically are not tolerant of sensor or actuator failures.

3) Inertial sensors and intrastructural actuators can be combined to achieve active isolation. The successful demonstration of the AIFs showed that active isolation can be achieved while preserving static stiffness. This differentiates these devices from others, which achieve isolation by reducing stiffness and adding damping to the (now much lower frequency) fundamental mode. The AIFs use simple off-the-shelf hardware to achieve 20 dB of broadband isolation.

4) The number of actuators and sensors used in a control system is a complicating factor in almost all test operations. The 30 sets of actuators and sensors we implemented was a significant implementation burden through most of the program. Although a reduction in the number of actuators would have been difficult to justify in view of the challenging performance goals, any designer of a less ambitious system should weigh carefully this aspect of design. In particular, approaches that attack disturbances at their source or at choke points (as was done with the six AIFs) usually employ fewer actuators than those that try to eliminate the vibrations once they have already entered the system.

The numerous additional lessons learned in connection with implementation and test of multivariable digital control designs will be discussed separately.

In summary, the research program has demonstrated active vibration control technology that reduces spacecraft-generated vibration transmitted to the payload by more than 20 dB over a broad frequency range and that damps payload components to remove resonant behavior. The capabilities of the active technology have been demonstrated clearly. The control system components are straightforward and well within existing flight capabilities. Moreover, the technologies are easy to retrofit using existing structure or interfaces.

## References

[1]Das, A., and Thompson, R., "Experimental Facilities for System Identification," *Proceedings of the USAF/NASA Model Determination for Large Space Structures Workshop*, Vol. 1, Jet Propulsion Lab., JPL-D-5574, California Inst. of Technology, Pasadena, CA, 1988, pp. 1–35.

[2]Sparks, D. W., Jr., and Juang, J.-N., "Survey of Experiments and Experimental Facilities for Control of Flexible Structures," *Journal of Guidance, Control, and Dynamics*, Vol. 15, No. 4, 1992, pp. 801–816.

[3]Waites, H. B., and Jones, V. L., "Cost Effective Development of a National Test Bed," *Proceedings of the Second NASA/DoD Control Structures Interaction Technology Conference 1987*, U.S. Air Force Wright Aeronautical Labs., AFWAL-TR-88-3052, NTIS, Springfield, VA, 1987, pp. 457–483.

[4]Quatararo, R., and Harris, J., "ASTREX—A Facility for Integrated Structures and Control Research," *Proceedings of the Second NASA/DoD Control Structures Interaction Technology Conference 1987*, U.S. Air Force Wright Aeronautical Labs., AFWAL-TR-88-3052, NTIS, Springfield, VA, 1987, pp. 364–375.

[5]Anon., "Controls-Structures Interaction Experiments for Large Space Structures Guest Investigator Program," NASA Research Announcement NRA 89-LaRC-3, June 1989.

[6]Smith-Taylor, R., and Tanner, S. E., *Controls Structures Interaction Guest Investigator Program: Overview and Phase I Experimental Results and Future Plans*, NASA TM-4412, 1993.

[7]Hyland, D. C., Longman, R. W., and Junkins, J. L., "Active Control Technology for Large Space Structures," *Journal of Guidance, Control, and Dynamics*, Vol. 16, No. 5, 1993, pp. 801–821.

[8]Hyland, D. C., King, J. A., and Phillips, D. J., "Streamlined Design and Self-Reliant Hardware for Active Control of Precision Space Structures," NASA CR 4637, NAS1-19372, Dec. 1994.

[9]Hyland, D. C., and Phillips, D. J., "Development of the Linear Precision Actuator," 11th Annual AAS Guidance and Control Conf., Keystone, CO, AAS Paper 88-067, Jan. 1988.

[10]Phillips, D. J., and Collins, E. G., Jr., "Four Experimental Demonstrations of Active Vibration Control for Flexible Structures," *Proceedings of the AIAA Guidance, Navigation, and Control Conference* (Portland, OR), AIAA, Washington, DC, 1990, pp. 1625–1633.

[11]Phillips, D. J., Hyland, D. C., Collins, E. G., Jr., and King, J. A., "The Multi-Hex Prototype Experiment," *Proceedings of the IEEE Conference on Decision and Control* (Brighton, England, UK), Inst. of Electrical and Electronics Engineers, New York, 1991, pp. 2024–2029.

[12]Hyland, D. C., Daubendiek, A. W., and Phillips, D. J., "System Identification of the Multi-Hex Prototype Experiment," *Proceedings of the American Control Conference*, Boston, MA, 1991, pp. 3013–3018.

[13]Anderson, B. D. O., and Vongpanitlerd, S., *Network Analysis and Synthesis: A Modern Systems Theory Approach*, Prentice-Hall, Englewood Cliffs, NJ, 1973.

[14]Benhabib, R. M., Iwens, R. P., and Jackson, R. L., "Stability of Large Space Structure Control Systems Using Positivity Concepts," *Journal of Guidance and Control*, Vol. 4, No. 6, 1981, pp. 487–494.

[15]Lozano-Leal, R., and Joshi, S., "Strictly Positive Real Transfer Functions Revisited," *IEEE Transactions on Automatic Control*, Vol. 35, Nov. 1990, pp. 1243–1245.

[16]Wen, J. T., "Time Domain and Frequency Domain Conditions for Strict Positive Realness," *IEEE Transactions on Automatic Control*, Vol. 33, Oct. 1988, pp. 988–992.

[17]Hyland, D. C., and Phillips, D. J., "Advances in Active Vibration Isolation Technology," *Proceedings of the 10th Virginia Polytechnic Institute and State University Symposium on Structural Dynamics and Control*, Blacksburg, VA, 1995, pp. 367–378.